Growth and Elongation Within and Along the Axon

Phillip Lamoureux,[1] Steven R. Heidemann,[2] Nathan R. Martzke,[1] Kyle E. Miller[1]

[1] Department of Zoology, Michigan State University, East Lansing, Michigan 48824-1115

[2] Department of Physiology, Michigan State University, East Lansing, Michigan 48824-3320

Received 3 August 2009; revised 18 September 2009; accepted 15 October 2009

ABSTRACT: Mechanical tension is a particularly effective stimulus for axonal elongation, but little is known about how it leads to the formation of new axon. To better understand this process, we examined the movement of axonal branch points, beads bound to the axon, and docked mitochondria while monitoring axonal width. We found these markers moved in a pattern that suggests elongation occurs by viscoelastic stretching and volume addition along the axon. To test the coupling between "lengthening" and "growth," we measured axonal width while forcing axons to grow and then pause by controlling the tension applied to the growth cone or to the cell body. We found axons thinned during high rates of elongation and thickened when the growth cones were stationary. These findings suggest that forces cause lengthening because they stretch the axon and that growth occurs, in a loosely coupled step, by volume addition along the axon. © 2009 Wiley Periodicals, Inc. Develop Neurobiol 00: 000–000, 2010

Keywords: **cytoskeleton; axonal transport; mechanical processes; growth cones; nerve regeneration; mitochondria**

INTRODUCTION

Recent studies of axonal elongation (i.e., growth involving increased axon length and net volume addition) have focused strongly on the behaviors, mechanics, and cytoskeletal events in the growth cone (Conde and Caceres, 2009; Lowery and Van Vactor, 2009). Although it is clear that force generation through an actin-based motor-clutch system at the leading edge of the growth cone is important for axonal elongation (Bard et al., 2008; Chan and Odde, 2008; Shimada et al., 2008), there are virtually no data on how forces lead to the formation of new axon (Goldberg and Burmeister, 1986; Mitchison and Kirschner, 1988; Lamoureux et al., 1989). Several studies over the years have suggested that markers along the axon, including branch points and fiduciary marks on the microtubule cytoskeleton, remain stationary during axonal elongation (Bray, 1970, 1973; Hirokawa et al., 1997). This led to the logical inference that the effects of force generation at the growth cone are confined to the growth cone (Mitchison and Kirschner, 1988). This is somewhat curious insofar as it is clear that extensive and rapid elongation of axons can be experimentally induced in response to tension without a contribution from the growth cone (Bray, 1984; Campenot, 1985; Abe et al., 2004; Pfister et al., 2004; Bernal et al., 2007; O'Toole et al., 2008a, b).

To begin addressing the question of how new axon is formed, we designed studies to observe and measure both of the basic aspects of axonal growth, these include length change per se and volume changes, within and along the axon. Using a variety of axonal markers, we find an entirely similar set of axonal "behaviors" during normal spontaneous axonal elongation and in response to experimentally applied tension. Our observations and experiments suggest that axons lengthen by viscoelastic stretching (e.g., simi-

Additional Supporting Information may be found in the online version of this article.

Correspondence to: K.E. Miller (kmiller@msu.edu).

Contract grant sponsor: Michigan State University (K.E.M.).

Published online in Wiley InterScience (www.interscience.wiley.com).
DOI 10.1002/dneu.20764

lar to slowly stretching "Silly Putty") in response to tension. This stretching is loosely coupled in time with intercalated addition of material along the axon.

MATERIALS AND METHODS

Cell Culture

Chick sensory neurons were isolated as described (Sinclair et al., 1988). Cells were grown and imaged at 37°C in L-15 medium (Sigma Chemical, St. Louis, MO) supplemented with 0.6% glucose, 1 m*M* glutamine, 100 U/mL penicillin, 136 μg/mL streptomycin sulfate, 10% fetal calf serum, 50 ng/mL 7S nerve growth factor (Harlan Bioproducts, Indianapolis, IN), and N9 growth supplement (Heidemann et al., 2003). The culture surface was treated with 0.01% polyornithine, rinsed, and treated with 20 ng/mL laminin. Mitochondria were labeled with 0.1 μM MitoTracker Red CMXRos (Invitrogen, Carlsbad, CA), incubated for 2 min, and recovered in fresh L-15 for 2 h (Miller and Sheetz, 2006). Cultures were maintained in a ringcubator (Heidemann et al., 2003) on the stage of a Leica DM IRB inverted microscope and observed with a N Plan L 40**x**/0.55 corr Ph2 with an adjustable collar infinity/0-2/c objective. Cells were illuminated with a 100 W Xenon lamp attenuated 98% with neutral density filters through a Texas Red cube (Chroma, Rockingham, VT) for visualization of MitoTracker.

Data Analysis

Images were taken with Openlab (Improvision, Waltham, MA) using a Orca-ER digital camera CCD, model#CA742-95 (Hamamatsu, Bridgewater, NJ), converted into TIFFs, and analyzed using ImageJ (NIH). Images were rotated using the ImageJ plug-in TJRotate and the StackReg macro was used to align each sequence of images as previously described (Miller and Sheetz, 2006). The images were then cropped, resliced, and z-projected to produce kymographs. Thirty-minute sections of the kymographs were used to track the mitochondrial positions by manual point selection.

Axonal Width Measurement

To automate the process of size analysis, we developed an ImageJ plugin (named "Width Measurement") that measures pixel intensity across objects, finds the derivative to determine the steepest points, and then calculates the distance between these points (O'Toole et al., 2008a, b). In phase contrast images, as light passes through a translucent objects, destructive and constructive inference patterns emerge that conventionally appear as dark regions with a bright halo. In previous work, we defined the edges of the axon to be at the steepest points in the intensity gradient at the border of the dark center and bright halo (O'Toole et al., 2008a, b). Our width measurement plugin uses the derivative of pixel intensity across the axon to find these steepest points and returns the distance between these points to calculate axonal width. To prepare images for analysis, images of axons acquired at 12-bit pixel depth were opened in ImageJ, converted to 32-bits, and straightened using the "Straighten" plugin (Kocsis et al., 1991). In this plugin, points along a curved object are manually selected, a nonuniform cubic spline is fitted to the points by the program, and the object is remapped from curved to a linear coordinates. This orients the axon, so that width measurements are made orthogonally instead of at random angles. The straightened image is then stretched 8x on the *y*-axis by interpolation using the ImageJ plugin TransformJ set to quintic B-spline (Meijering et al., 2001). This plug-in uses a more sophisticated algorithm than the built-in ImageJ rescaling function, which smoothly rescales the size of the image. To remove high frequency noise, a Gaussian Blur filter with a radius two pixels was applied using the built-in ImageJ function. The width measurement plugin was then run to determine axonal width at each pixel along the axon. The source code for the plugin is available on request.

Towing Procedure

Micropipettes were calibrated for their bending spring constant and coated with polylysine and concanavalin A (1 mg/mL) as previously described (Heidemann et al., 1999). A calibrated needle and reference needle were held in a double needle holder by a hydraulic micromanipulator and the growth cone of the neuron was manipulated onto the towing needle. The manipulator was then used to exert axial tension on the axon and the force applied was determined from the bending of the calibrated needle relative to the reference needle. The resulting axonal lengthening response is referred to as "stretch" here, for the sake of simplicity. It is more accurately described by the engineering term "creep," which is a plastic deformation in response to force. Such a fluid-like deformation is familiar from the "stretching" of clay or Silly Putty, in which the material does not elastically recover the deformation upon the cessation of force, which is dissipated by the deformation.

Bead Movement

One micrometer polystyrene beads (Sigma) were treated with a 5% polyethyleneimine (Sigma) for 30 min, then spun down, and rinsed twice with distilled water. The pellet was resuspended and an aliquot diluted fivefold. From this diluted stock solution, 20 μL aliquots were repeatedly administered in the vicinity of a rapidly growing DRG axon to ensure beads were bound throughout the observation/growth period. The cultures were warmed in a ringcubator stage heater (Heidemann et al., 2003) and grown in L-15 media. Time-lapse digital images were collected with an Orca-ER cooled CCD camera using the OpenLab Improvision program. Figure panels and the kymograph were made with ImageJ and finally composed in Photoshop.

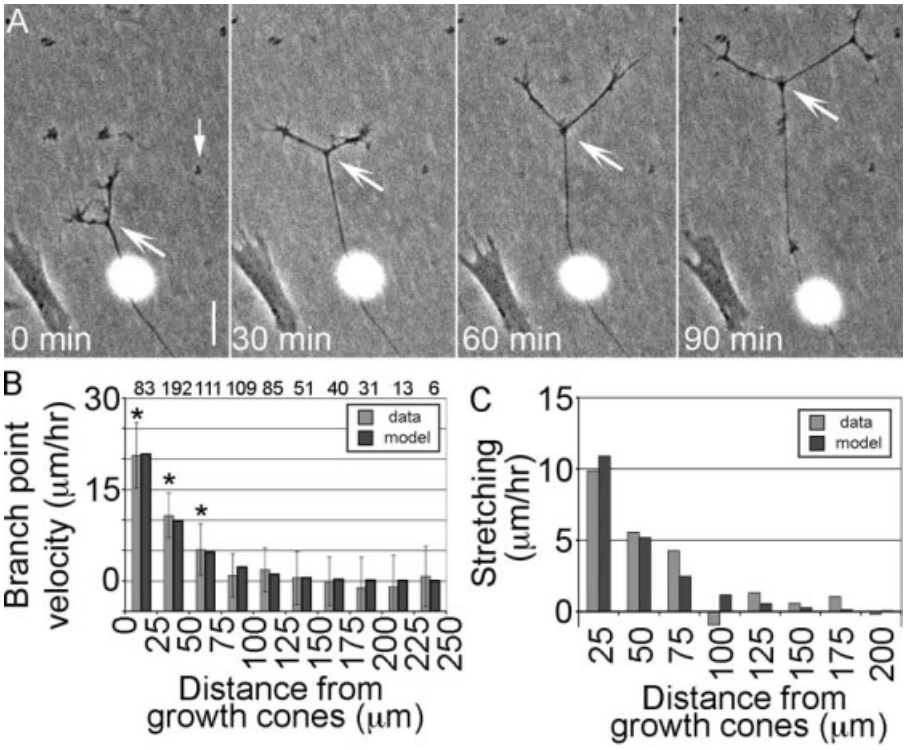

Figure 1 Axonal branch points advance in a pattern consistent with axonal stretching. A, The movement of an axonal branch point is shown in a series of time lapse images (Video 1). The thick arrows point out the branch point and the thin arrow points to a stable reference point; bar = 20 μm. B, Branch point movements, over 30-min time intervals, were pooled into 25-μm bins based on the average distance of the branch point from the growth cones. The boundaries of each bin are listed on the *x*-axis of the graph. The error bars show the 95% confidence intervals and the number of branch points in each bin is listed along the top of the graph. The asterisks indicate regions along the axon where significant forward movement occurred ($p < 0.05$). The dark bars show the fitted velocity profile of branch point movement based on our theoretical model of axonal stretching (O'Toole et al., 2008a, b). This model incorporates force generation at the growth cone, the viscosity of the axon, and the strength of adhesions along the axon to predict movement along the axon as the result of axonal stretching. C, A comparison of the observed and predicted amount of axonal stretching over 25-μm regions and 30-min time intervals plotted against the average distance from the growth cones.

All animal studies were approved by the Michigan State University Institutional Animal Care and Use Committee.

RESULTS

Axonal Branch Points Advance in a Pattern Consistent with Stretching During Axonal Elongation

We were motivated to reconsider the growth responses of axons to tension in greater detail by what were initially serendipitous observations of branch point movements in chick sensory neurons [Fig. 1(A) and Video 1], which contrasted with earlier observations as outlined in the Introduction section. To determine whether such branch point movement is a frequent or atypical behavior, we analyzed the velocity of 103 branch points arrayed along 30 spontaneously growing neurons. The position of branch points along the axon were binned into 25-μm intervals (from the growth cone) and their movement measured during 30-min time intervals; in total, 721 measurements were made. As shown in Figure 1(B), branch points within 100 μm of the growth cone showed a statistically significant forward velocity. We interpret this as stretching for three reasons.

First, the drop in velocity along the axon indicates that points along the axon are moving apart. For example, branch points that were between 0 and 25 μm from the growth cone moved at an average velocity of 20 μm/h, whereas branch points 25 to 50 μm

Table 1 Effect of Mitotracker and Fluorescent Illumination on Axonal Elongation

Fluorescent Illumination	Mitotracker	Rate of Elongation (m/h ± SD)	Cells (*n*)	Growth Cones (*n*)
None	No	35 ± 19	8	12
None	Yes	35 ± 21	3	5
2 min intervals	Yes	34 ± 18	10	34
2 s intervals	Yes	31 ± 11	6	11

To determine whether treatment with Mitotracker or fluorescent illumination disrupted axonal elongation, sensory neurons were plated as described in the Methods section and phase images were acquired at regular intervals. Application of Mitotracker and fluorescent illumination was varied as noted in the table.

from the growth cone moved at an average velocity of 10 μm/h [Fig. 1(B)]. Thus, over the course of an hour, 10 μm of elongation occurred in this region of the axon [Fig. 1(C)]. Second, our previous work with chick sensory neurons indicates that their axons are under tension, not compression, thus the increase in distance of points along the axon is the net result of pulling forces that "stretch" the axon as opposed to pushing forces that "telescope" the axon (Lamoureux et al., 1989; O'Toole et al., 2008a, b). Altogether, we found that 352 of our 721 observations showed a velocity greater than 5 μm/h. Indeed, 46 observations showed branch points moving at or above 40 μm/h, the average rate of growth cone advance for this cell type (Table 1). Finally, these data closely match our published quantitative model of marker movement based on stretching in response to tension (O'Toole et al., 2008a, b). This models net axonal elongation as a function of force generation at the growth cone, axonal viscosity, and strength of axonal adhesions. As shown in Figure 1(B,C), both the velocity gradient [Fig. 1(B)] and the pattern of stretching over the distal 100 μm [Fig. 1(C)] closely match the prediction of the mathematical model. Taken together, these data suggest tension generated at the growth cone causes axonal lengthening by stretching of the axonal framework.

Movement of Beads Also Indicates Axonal Stretching during Normal Elongation

We wished to determine whether our observations using branch points as markers for axoplasmic movements could be confirmed by using beads bound to the axon. This technique has a long history for monitoring the surface movements of both the actin cortex and the flow of the plasma membrane (Bray, 1970; Smith, 1988; Zheng et al., 1991; Okabe and Hirokawa, 1992; Suter et al., 1998). Of note, 0.5-μm beads coated with rat IgG diffuse freely in the membrane and track the flow of the plasma membrane (Dai and Sheetz, 1995), whereas 1-μm glass or polystyrene beads treated with polyethyleneimine are coupled to the actin cortex and serve as markers for its motion. These beads have the advantage that they can be used on unbranched axons, thus simplifying velocity measurements compared to branch points at different angles, and confirming that the movement is truly general and not merely relevant to a subset of axonal branch points.

We found that the beads moved in a manner entirely consistent with the branch points (Fig. 2 and Video 2). Figure 2(A) shows a typical observation. Figure 2(B) shows a kymograph (Miller and Sheetz, 2006) of this neuron allowing the bead movements to be easily tracked through time and for velocities of bead movements to be measured. Figure 2(C) shows the analysis of bead movements for 13 neurons with 40 growth cones among them. As was seen with the movement of the branch points, beads bound to regions of the axon within 100 μm of the growth cone showed statistically significant velocities and this profile is again consistent with the model of O'Toole et al. (2008). At any given time, therefore, the axon has a distal-most bead some distance behind the growth cone. Using this as a marker, we found that 35 to 80% of the overall increase in length of the axon resulted from increased distances between the cell body and the distal-most bead. That is, of the total axonal lengthening between the cell body and growth cone (100%) during a given period, some 35 to 80% of it occurred as a result of intercalated lengthening in the proximal region between the cell body and a bead located well behind the growth cone.

Stretching of the Axonal Framework Occurs at All Rates of Growth Cone Advance

Although movements suggesting stretching have been observed in *Xenopus laevis* neurites, this has been regarded as an artifact of their rapid elongation that can be as high as 200 μm/h (Baas and Brown, 1997; Chang et al., 1998). Although the rate of embryonic sensory neuron elongation is much slower ($\sim$35 μm/h, Table 1), the earlier interpretation suggests the possibility that the stretching indicated by branch point (Fig. 1) and bead movement (Fig. 2) may simply be the result of occasional periods of "rapid" growth cone advance. To answer this

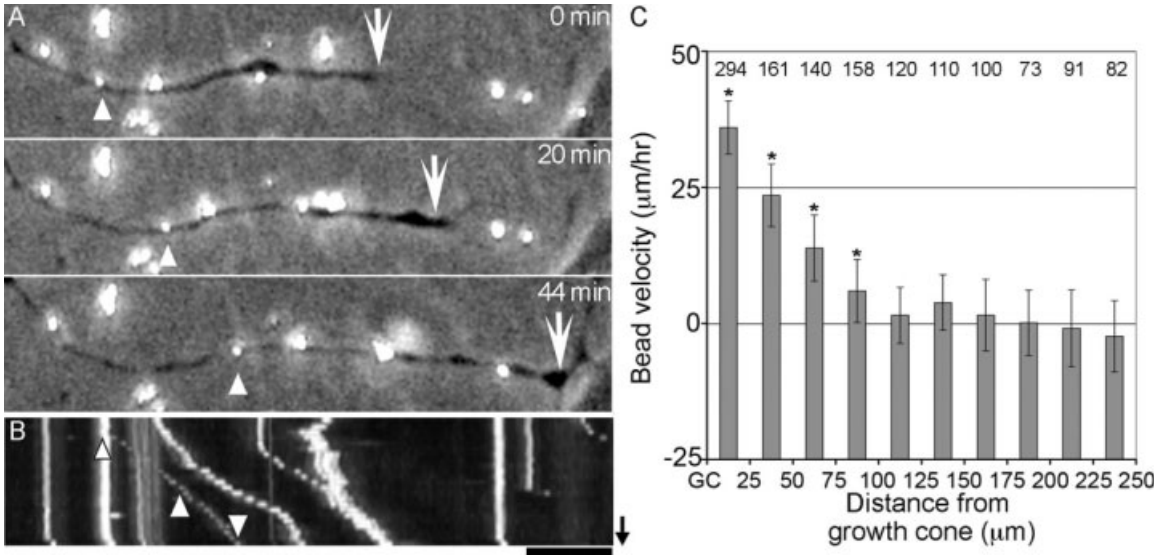

Figure 2 Beads bound to the cortical actin cytoskeleton advance in a pattern consistent with axonal stretching. A, Movements of 1-μm polystyrene beads bound to an axon (bright white spots) are shown in a series of phase time-lapse images (Video 2). Triangles and arrows, respectively, track a bead and the growth cone. B, A kymograph of the phase images shows the advance of multiple beads attached to the axon (diagonal white lines). The bead noted in panel A is labeled with white triangles; black arrow = 10 min; bar = 10 μm. C, Bead movements were pooled into 25-μm bins (the boundaries of the bins are listed on the *x*-axis of the graph) and plotted against the distance from the growth cone (average ±/ 95% confidence interval). Asterisks mark significant bead advance ($p < 0.05$). The numbers of observations for each bin are shown along the top of the graph.

question, we monitored the movement of mitochondria "docked" to the axoplasmic matrix in axons [Fig. 3(A) and Video 3] that were undergoing different rates of normal axonal elongation (Miller and Sheetz, 2006; O'Toole et al., 2008a, b). Docked mitochondria were classified as those that moved slower than 0.1 μm/s (i.e., 360 μm/h), a rate that is considered to be the lower limit of kinesin- and dynein-mediated fast axonal transport (Brown, 2003). Using kymographs to examine the velocity of docked mitochondrial movement along the axon [Fig. 3(B)], we determined the velocity of docked mitochondrial movement over 30-min time periods for the 10-μm region of the axon that was 50 μm from the growth cone. We then compared the velocity of docked mitochondrial movement with the rate of growth cone advance [Fig. 3(C)]. In the graph, it can be seen that forward movement of docked mitochondria occurred at all rates of normal axonal elongation. Focusing on the slowest rates of elongation (i.e., between 0 and 10 μm/h), the average rate of mitochondrial movement in the 10-μm region 50 μm from the growth cone was 6.4 ± 2.5 μm/h (average ± 95% confidence interval [CI], $n = 34$ observations). Using a two-tailed *t* test to determine whether there was a significant difference between the observed motion and a hypothesized average velocity of zero, we found that there was significant movement ($p < 0.0001$). These data suggest that axonal stretching is not an artifact of high rates of growth cone advance.

Equivalent Axonal Stretching Occurs in Response to Experimentally Applied Tension

We previously termed the movements of docked mitochondria such as that of Figure 3 as "low velocity transport" (LVT) and hypothesized that it was due to tension exerted at the growth cone (Miller and Sheetz, 2006). We tested this hypothesis by observing the movements of mitochondria in response to mechanical tension directly applied with a microneedle, as shown in Figure 4 and Video 4. In these experi-

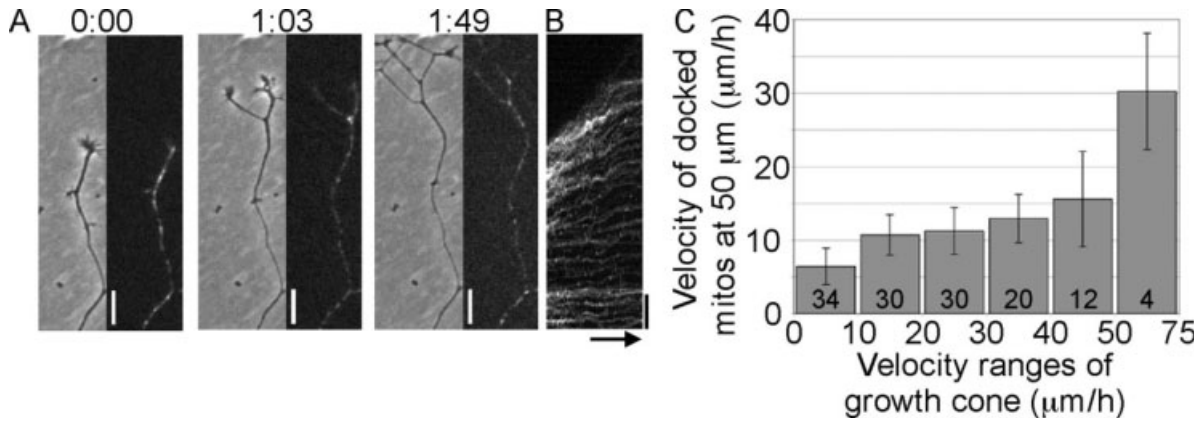

Figure 3 Axonal stretching occurs at all rates of growth cone advance. A, Matched phase images of axons and fluorescent images of axonal mitochondria during normal growth (Video 3). B, A kymograph (bar 20 μm, arrow 1 h) shows that docked mitochondria advance and spread apart. C, Comparison of the velocity of the growth cone and the velocity of docked mitochondrial movement 50 μm from the growth cone demonstrates that axonal stretching occurs at all rates of growth cone advance. The data were grouped into bins based on the rate of growth cone advance, the numbers on the *x*-axis are the lower and upper bounds for each bin. The error bars are the $\pm$ 95% confidence intervals and the number of observations in each bin are listed at the bottom of the bars.

ments, we routinely towed axons at rates above and below typical growth cone-advance rates, i.e., above and below 35 μm/h (Table 1). The kymograph in Figure 4(B) shows an example of the effect of this on the movement of mitochondria. As can be seen from the change in the "slope" of the mitochondria in the kymograph, the rate of mitochondrial movement is proportional to the rate of experimentally induced elongation. We applied this experimental design to 30 axons and tracked the movement of a total of 315 mitochondria. We then divided the data into conditions where we towed at greater than or less than 35 μm/h. Analysis of these data, Figure 4(C), indicates that the stretching rates decline in the same characteristic exponential pattern with distance from the distal end of the axon for both stretching in response to experimental tension and as a result of growth cone advance, as seen in the Figures 1–3. These data suggest that axonal stretching and LVT-type mitochondrial movements are the result of tension on the axon. Further, these data demonstrate that significantly higher rates of movement occur under conditions with higher rates of forced axonal elongation. In addition, they show that when axons are towed at their normal rate of growth, the movement of mitochondria along the axon is not significantly different from what is observed during normal elongation. The data presented thus far indicate that the axon stretches at all rates of lengthening.

Axonal Caliber Recovers in an Intercalated Manner Following Axonal Elongation

Given the evidence that axons behave as viscoelastic solids over the time scale of minutes (Dennerll et al., 1989), we would expect that stretching of the axon would lead to a decrease of axonal diameter over short time scales. If the elongation represented true growth, however, axonal diameter would then recover over longer time scales as the axon adds mass. Figure 5 shows one example of this phenomenon in a normally growing neuron with two branches over the course of 8:20 h. The branch to the left initially thinned during 3:20 h of growth (empty arrows). During the next 5 h of growth, however, it thickened (full arrows), whereas the other branch thinned (triangles).

The considerable variability in growth cone-mediated elongation over time and in the affected region that undergoes stretching made it difficult to conduct quantitative studies of thinning and thickening during normal elongation. Consequently, we analyzed the extent and time scale of thinning and subsequent recovery in our regime of experimental towing of axons. We rapidly elongated the axon to maximize stretch (Video 6), per our results above, and then held the axon at this length for some hours [Fig. 6(A,B)] to observe recovery if any. We also attempted to

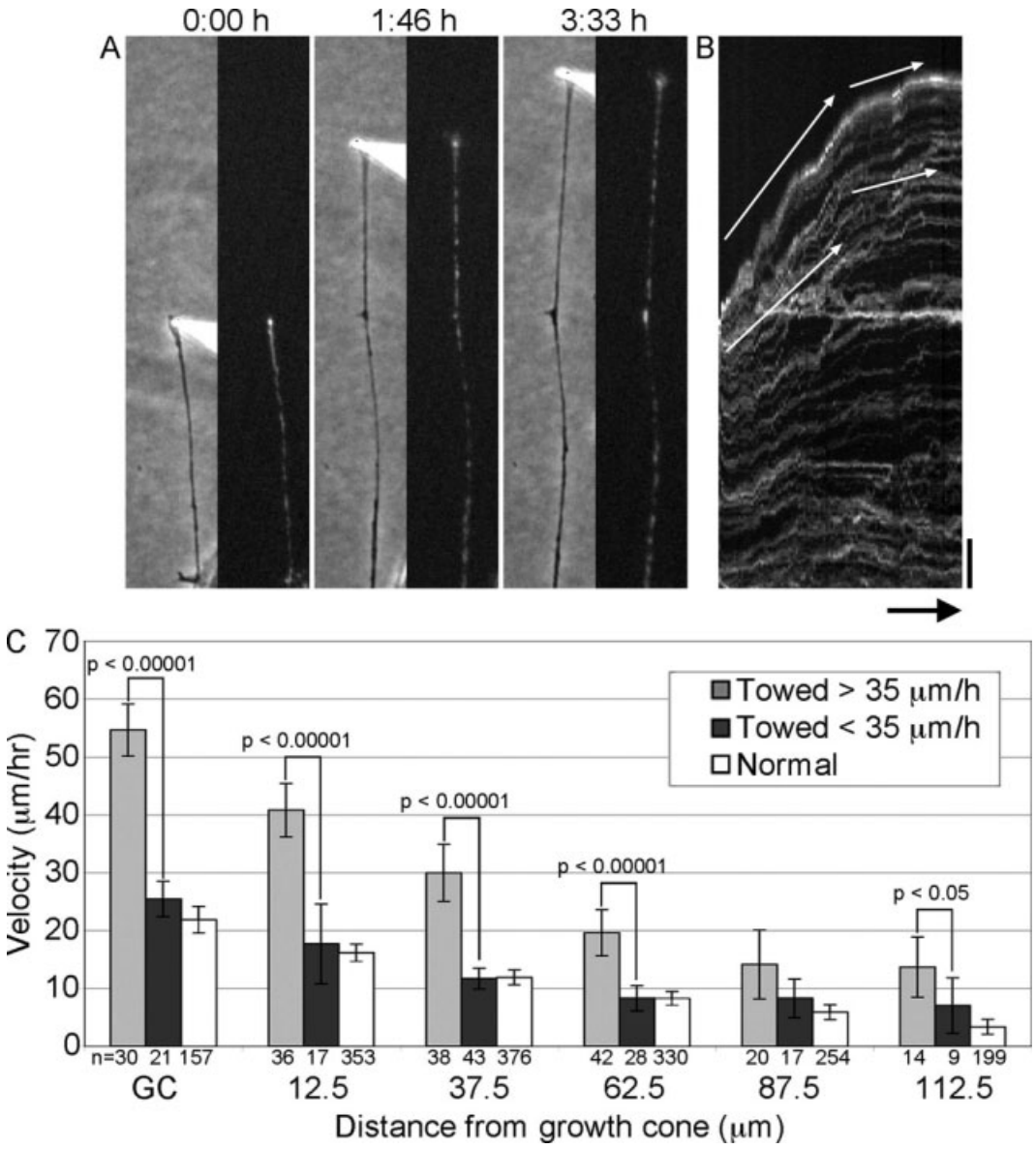

Figure 4 Docked mitochondria move in a pattern consistent with axonal stretching during towed growth. A, Matched phase images of axons and fluorescent images of axonal mitochondria during towed growth (Video 4). To analyze the effect of forces on LVT, the growth cone was initially towed with high force at a rate of $\sim$50 μm/h for $\sim$1:30 h and then with low force at a rate of $\sim$5 μm/h for $\sim$1:30 h. B, A kymograph (bar 20 μm, arrow 1 h) shows docked mitochondria along the axon advancing and spreading apart. The differences in towing velocity are reflected in the differences in docked mitochondrial movement shown by the white arrows on the kymograph. The rates of movement 50 μm from the tip of the axon for the low and high force conditions were 8 and 28 μm/h, respectively. C, To determine quantitatively if forces applied at the growth cone influence docked mitochondrial movement, axons were towed at high (> 35 μm/h) and low rates (< 35 μm/h) and mitochondrial movement was observed. As a control, we included the rates of mitochondrial movement observed during growth cone mediated elongation. To analyze the data, the movement of individual mitochondria over 30-min time periods was measured. The number of observations is shown under each bar at the bottom of the graph. The velocity of mitochondrial movement was significantly higher when towing occurred at rates > 35 μm/h as compared to when towing at <35 μm/h; the significance levels are shown on the graph. The error bars are the 95% confidence intervals.

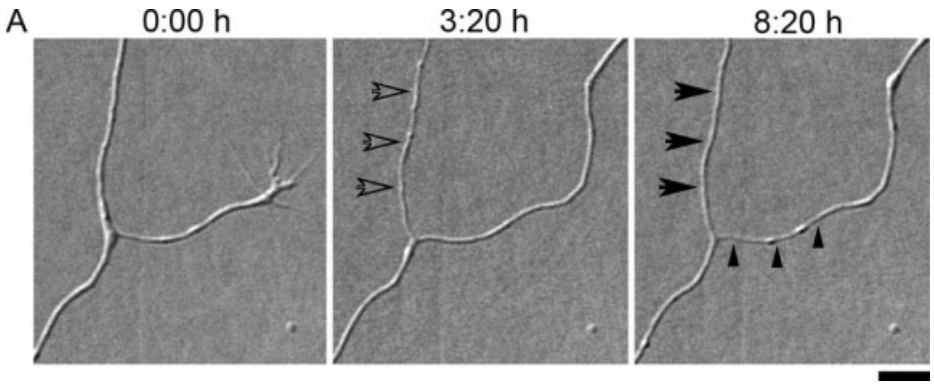

Figure 5 Axons thin and thicken during normal axonal elongation. A, Two branches of a growing neuron are shown over the course of 8:20 h. The branch to the left initially thinned during 3:20 h of growth as illustrated with the open arrows. During the next 5 h of growth, this branch thickened (filled arrows) and the right branch thinned (black triangles); bar = 20 μm.

attach the elongated axon to the dish for longer periods of recovery. Analyses of recovery of axon caliber were conducted by an automatic method for measuring diameters accurately using the width measurement plugin we developed in ImageJ.

Figure 6(D) shows the quantitative stretch and recovery data from the same neuron shown in 6B, which is shown at 8-fold expansion in 6C for clarity. Figure 6(D) shows that the axon was initially 140-μm long and was experimentally elongated over the course of 2 h to a length of 310 μm causing the thinning/caliber reduction seen in the figure. However, over the course of the next 18 h, the caliber recovered, and the growth cone advanced slightly. Notably, caliber recovery was rather uniform along the length of the axon. In so doing, the volume increased from 422 to 1023 μm^3 (assuming a circular cross section). Figure 6(D) shows the combined data from similar experiments at both short ($\sim$5 h) and long ($\sim$20 h) recovery times. In both cases, the experimentally induced thinning and the subsequent recovery were statistically significant. Nevertheless, the data from the longer recovery periods indicate a larger recovery of axon caliber.

Mitochondria Add Along the Length of the Axon to Maintain Mitochondrial Density

At the extreme, the changes in axonal diameter and volume shown above could occur simply by loss or gain of axoplasmic water. Consequently, we wished to examine the addition of mitochondria, a functional component of the axon that is discrete and can be counted. We monitored the addition of fluorescently labeled mitochondria to the axonal shaft while taking images every 2 min for several hours. Figure 7(A) is an example that demonstrates that net axonal fluorescence increases over the course of 3 h of elongation. Visual evidence of mitochondrial addition to the axon is indicated by the white arrows.

To test whether mitochondrial addition to the axonal shaft also occurred following experimental application of external forces, we towed growth cones, reattached them to non-neuronal cells on the dish, and then waited several hours. We found decreased mitochondrial density along the axon following a rapid elongation and then increases in mitochondrial density along the axon during extended growth cone pauses or recovery from applied stretch [Fig. 7(B) and Video 6]. These experiments demonstrate that mitochondrial addition is not restricted to the growth cone, but rather can occur along the axonal shaft.

It is well established that the axons of sensory neurons elongate without thinning during both normal axonal elongation and in response to applied forces. (Bray, 1984). In contrast, axonal stretching is associated with axonal thinning (Popov et al., 1993). As we observed stretching in sensory neurons, we felt it was important to determine whether the neurons in our culture system thinned during elongation over the course of days. To test this, we monitored the total number of mitochondria added to the axonal arbors of 18 single neurons at 24 h intervals. Each neuron was identified at the beginning of the experiment by circling the dish beneath the neuron with a diamond "objective." The mitochondria were freshly labeled each day using MitoTracker several hours before the experiment. Total axonal length, mitochondrial linear density, and mitochondrial number were acquired on three successive days from three separate platings of

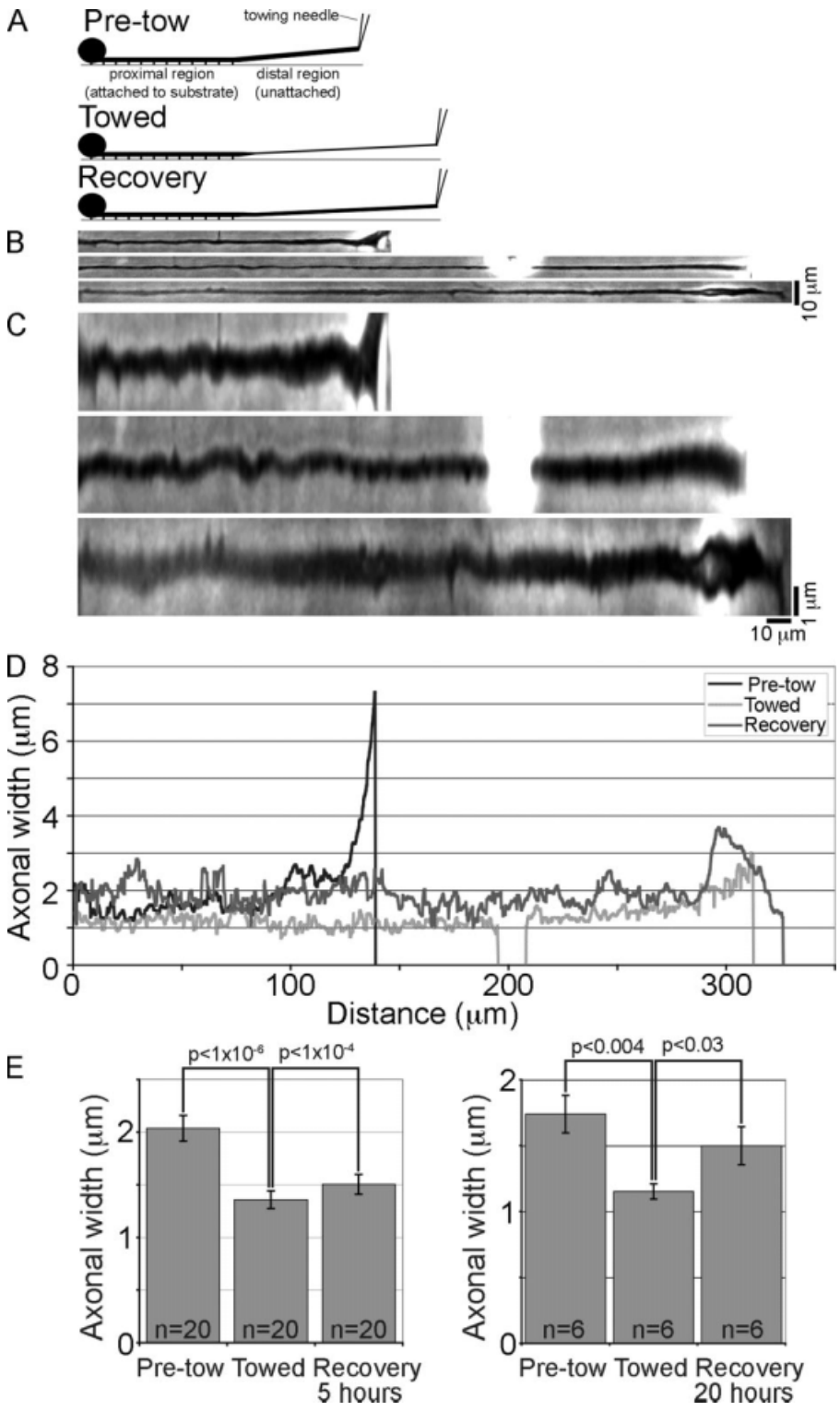

Figure 6 Mass addition occurs along the axon after forced elongation. A-C, Growth cones are towed at high rates (50-100 μm/h) and then held in position on the needle or reattached to the substrate. B, An example of a neuron that was rapidly towed for 2:45 h, reattached to the substrate, and allowed to recover for 18 h (Video 5). These images were straightened using the Straighten plugin in ImageJ. C, An 8x enlargement on the *y*-axis is shown to better visualize the initial thinning and recovery in axonal width. D, A graph of axonal width, generated by our automated Width Measurement tool, illustrates thickening occurs over the entire stretched region. E, Quantitative analysis demonstrates axonal width decreases significantly during rapid towing and then increases significantly during both short and long recovery periods. The significance levels are shown above the graph and the number of neurons analyzed in each condition are shown at the bottom of the graph. The graph shows the average $\pm$ SEM.

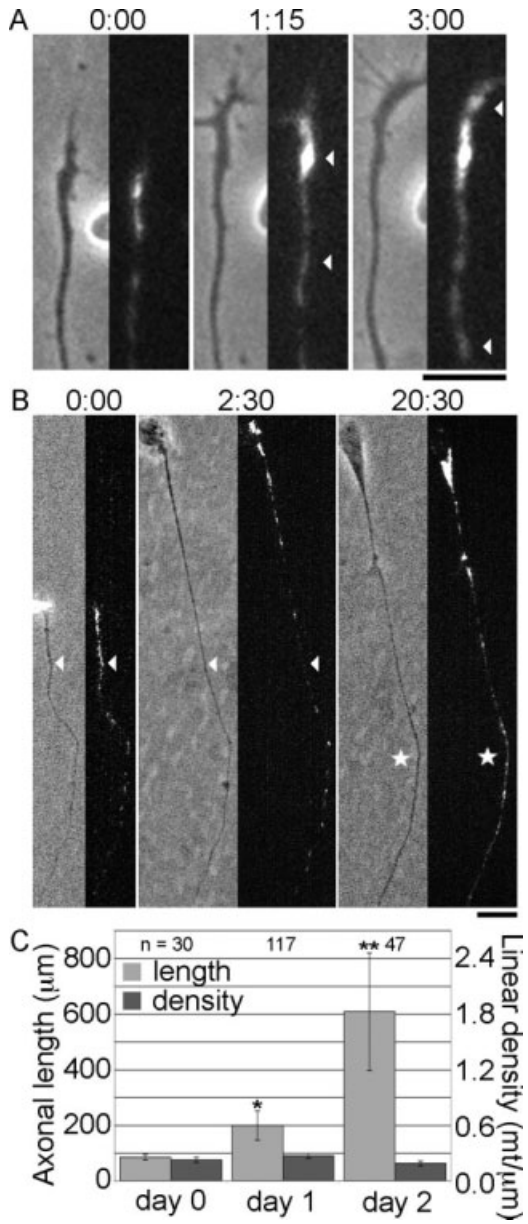

Figure 7 Mitochondrial addition occurs along the axon. A, Matched pairs of phase and fluorescent images of mitochondria during 3 h of growth cone-mediated elongation. The triangles point to sites of new mitochondrial addition; bar 20 μm. B, Matched pairs of phase and fluorescent images show a decrease in mitochondrial density during rapid towed growth (triangle) and then mitochondrial addition along the axon during an extended recovery period (star); bar 20 μm (Video 6). C, Axonal length and mitochondrial density where measured to determine if mitochondria were added to the axon during normal elongation (average $\pm$ 95% CI). The number of neurons analyzed on each day is shown at the top of the graph. As compared to Day 0, there were significant increases in axonal length (*$p < 0.05$; **$p < 0.0005$), but no significant changes in mitochondrial density.

sensory neurons over 3 weeks. As seen in Figure 7(C), the axons elongated from approximately 100 μm to 600 μm over 2 days but mitochondrial density remained constant at about 0.27 mitochondria/μm (no significant differences were observed between Day 1 and Days 2 or 3 using a two-tailed *t* test). A strong support for the stability of mitochondrial density during growth came from the small variance in mitochondrial density, in sharp contrast to the typically wide variability in axonal outgrowth itself. Thus, we confirm that neurons elongate without thinning over the course of days (Bray, 1984; Abe et al., 2004; Pfister et al., 2004; O'Toole et al., 2008a, b).

Tension Applied at the Cell Body Causes Proximal Axon Stretching and Growth

Previous investigations of tension as a stimulator of axonal development suggest that the axon is capable of elongation anywhere along its length (Abe et al., 2004; Campenot, 1985; Pfister et al., 2004). However, the data here, and most other data of axonal growth, indicate nearly all growth is occurring distally, perhaps implying a "forward polarization" of axonal elongation. To test more directly whether growth is possible anywhere along the axon and that distal growth is simply the result of distal tension, we "towed" neurons from their cell body and made the same measurements for stretching and axonal growth as above (Fig. 8 and Video 7).

Eight neurons were fluorescently labeled to observe their mitochondria and then towed from their cell body away from the growth cone, which we called a "reverse tow." All eight produced a kymograph of fluorescent mitochondria that showed proximal stretching in the mirror-image pattern of axons towed from the cell body: most extensive and rapid movements occurred near the cell body with exponential decay more distally. In four experiments, we successfully observed a recovery period following towing allowing measurements of axon caliber before, after, and following recovery of varying duration (Table 2). (The other four axons failed for various reasons, e.g., the cell body did not remain attached to the towing needle at the end of the tow.)

Figure 8 shows the results (Neuron 1 of Table 2) of such a reverse tow in a region of an axon that was 179 μm from the cell body and 379 μm from its growth cone prior to towing [Fig. 8(A) "Before"]. This cell body was "reverse towed" 152 μm over 6.5 h [Fig. 8(A) "After"]. As seen in Figure 8(B), the fluorescently labeled mitochondria in this region

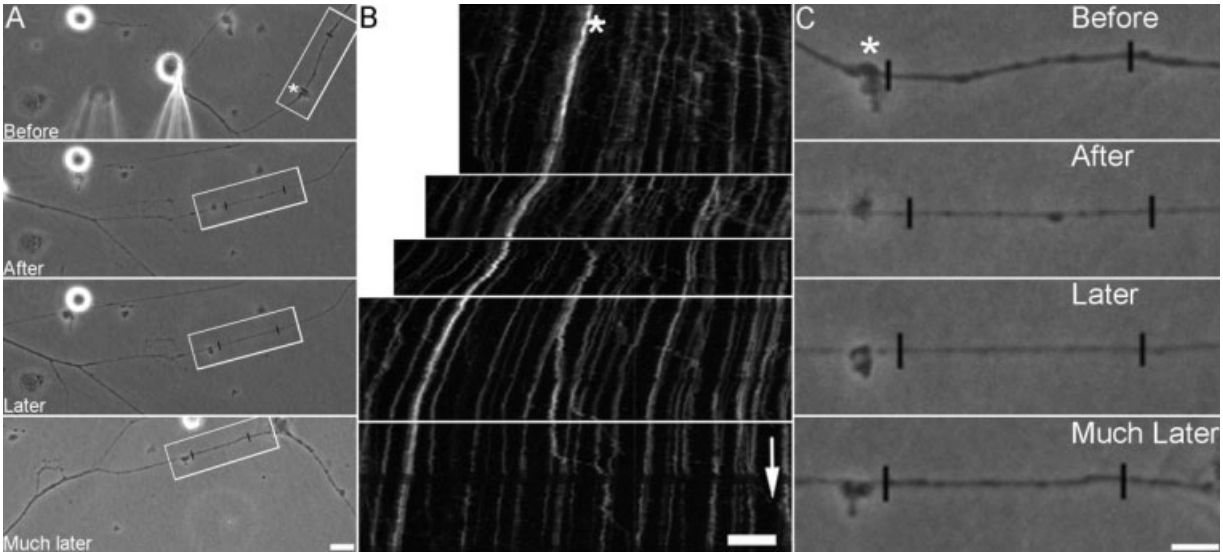

Figure 8 Stretch and recovery in response to tension applied at the cell body. A, Neuron (1 in Table 2) is shown at the four key time points: prior to the application of tension to the cell body, after 6.5 h of towing, after a recovery period of 2 h (Video 7), and much later (18.5 h). Boxes around axon show the specific axonal regions shown in panel C. The asterisk identifies cellular debris on the axon that served as a convenient marker throughout this particular experiment. B, A montage of kymographs of movements of fluorescent mitochondria in response to towing of the cell body (to the left) in the approximate axonal region outlined by the boxes in panels A and C. The montages were generated to correct for rotation of the boxed region over time. The "after" time point is at the top of the last section of kymograph and the "later" time point is at the bottom of this section; arrow length = 1 h and bar = 20 μm for all panels. C, The 50-μm region used for the width measurements in Table 2 is shown exactly by the black vertical lines on the phase images.

showed the same characteristic exponential decay of movement as had the distal regions in the earlier observations and experiments (Video 7). Phase images of axon caliber from this region before (8C "Before") and after (8C "After") towing, and then following 2 h (8C "Later") and an additional 10 h [Fig. 8(C) "Much later"] of recovery give the visual impression of initial thinning followed by recovery of axonal caliber. This is confirmed by diameter and area measurements shown in Table 2. In all cases, these measurements were taken from a 50-μm region in the middle of the axon.

DISCUSSION

Mechanical tension is well described to be an effective stimulus of axonal elongation and growth (Bray, 1984; Lamoureux et al., 1989; Pfister et al., 2004; Bernal et al., 2007). However, the growth/elongation

Table 2 Stretch and Recovery in Response to Tension Applied at the Cell Body

	Before Towing	After Towing	Recovery (Later)	Recovery (Much Later)	Distance from Cell Body (μm)	Distance from Tip (μm)
Time (h)	0	5.5	8	18		
Neuron 1	1.34 ± 0.04	1.20 ± 0.05	1.14 ± 0.05	1.25 ± 0.03	179	379
Neuron 2	1.35 ± 0.02	1.31 ± 0.02	1.42 ± 0.01	1.80 ± 0.05	50	400
Neuron 3	1.29 ± 0.03	1.20 ± 0.03	1.44 ± 0.05	NA	60	240
Neuron 4	1.18 ± 0.05	1.20 ± 0.04	1.25 ± 0.06	NA	110	170

Axonal diameter was measured immediately before towing and then at three later time points. Each of the values in the table is the average of 100 measurements made along 50-μm segments of the axon using the width measurement tool. The average time of the measurements is in the first row and the numbers in the first four columns are the average widths in units of μm ± 95% CI over 50-μm regions of the axon. The position of the measurement site in terms of distance from the cell body and the growth cone is given in the last two columns.

responses along the length of the axon in response to tension have received little or no attention. Most models view axonal elongation, either tacitly or explicitly, as being coincident with assembly of new axon, primarily at the growth cone often emphasizing microtubule assembly (Conde and Caceres, 2009; Lowery and Van Vactor, 2009). Here, we monitored the movement of axonal branch points, beads bound to the surface of the axon, and docked mitochondria. We found that during both normal axonal elongation and in response to applied forces axonal branch points, beads bound to the axon, and dock mitochondria moved in a pattern consistent with axonal stretching. By monitoring the width of the axons and the density of mitochondria, we found evidence that suggested axonal formation occurs through the assembly/deposition of new materials along the length of the axon. Our observations suggest axonal elongation involving two steps of differing "time constants": lengthening by stretching and growth by mass addition along the axon.

Our observation of axonal stretching is not surprising in itself given the evidence that axons behave as viscoelastic fluids, like clay or putty, over the time scale of tens of minutes (Dennerll et al., 1989; O'Toole et al., 2008a, b). What is surprising is the site of the stretching and axonal formation. Previous work examining axonal branch points and surface-adherent beads suggested that these markers were stationary along the axon and concluded that the act of assembly of new axon was directly linked to the advance of the growth cone (Bray, 1970, 1973). Here, we report branch points (Fig. 1 and Video 1), beads (Fig. 2 and Video 2), and docked mitochondria (Fig. 3 and Video 3) reveal stretching during spontaneous outgrowth in response to tension at the distal end of the axon. Similarly, we observed stretching in proximal regions when tension was applied to the cell body (Fig. 8 and Video 7). As noted earlier, this profile of growth activity reflects the predicted physical limitation of tension to the regions of the axon near the source of tension and as a result of adhesions to the substrate (O'Toole et al., 2008a, b). We also found that stretching along the axon occurs at all rates of elongation (Fig. 3). This is significant in that stretching of the axon during elongation has previously been observed in *X. laevis* neurons but was thought to be a peculiarity of their high rate of elongation, essentially an artifact of tension unrelated to normal growth (Popov et al., 1993; Chang et al., 1998).

As noted above, stretching of the axon during elongation had been observed earlier but was thought to be unique to *X. laevis* neurons. This raises the question of why the stretching and intercalated growth we observed so routinely was not also observed more generally by others. We think that part of the answer, at least, is that the two ends of the neuron, i.e., the growth cone and the cell body, commanded so much attention that the full length of the axon was simply overlooked. Nearly all of the reports of stationary markers during elongation were not investigations of growth responses per se but were designed as tests of the "structural hypothesis" of slow axonal transport (Baas and Brown, 1997; Hirokawa et al., 1997). Insofar as this model postulates assembly of the cytoskeletal network at the cell body and its transport as a contiguous structure down the axon, attention was focused on markers in the proximal regions of the axon. This is consistent with our results in that we too observed little or no axonal stretching/marker movement in the proximal third to half of the axon in response to tension at the distal end. Second, the emphasis on the growth cone as the highly dynamic, motile cell compartment guiding axonal elongation also deflected attention from the axon itself, e.g., possibly diminishing interest in an early report of intercalated growth (Campenot, 1985). Here, however, we see a bit of a paradox. Growth cone advance has been described by the influential "protrusion, engorgement, and consolidation" model of Goldberg and Burmeister (1986). It was originally proposed as a model for axonal growth, as indicated by the title "stages of axon formation," in which "assembly" of new axon occurs primarily at the growth cone leading to a pushing mechanism for growth cone advance. Subsequent data clearly showed that the growth cone advances by pulling (Lamoureux et al., 1989; Chada et al., 1997; Suter et al., 1998) causing axonal elongation (Lamoureux et al., 1989; Zheng et al., 1991). Although "protrusion, engorgement, and consolidation" has proven a productive model for understanding growth cone dynamics and locomotion, it is ironic that the original topic, stages of axon formation, subsequently received almost no direct investigation.

The movement patterns of axonal branch points, beads, and docked mitochondria all suggest that axonal formation occurs by axonal stretching. However, bona fide axonal growth, in our opinion, must include the addition of new mass to the axon. During ordinary growth cone-mediated elongation, we found that the density of mitochondria along the axon remained stable over 2-day periods while the axons increased in length by 6-fold (Fig. 7). These data strongly suggest mass addition is occurring along the axon during normal elongation; otherwise, the density of mitochondria along the axons would be six times smaller.

When we directly monitored changes in axonal diameter, we found that axons could both increase and decrease in diameter during growth cone-mediated axonal elongation (Fig. 5). To directly test whether volume increases occurred in stretched regions of the axon, we forced the axons to elongate by the application of tension to the growth cone while monitoring mitochondrial density and axonal width. We found the axons thinned when rapidly stretched at a rate of ~ 100 μm/h (Video 5) and then increased in width along the entire stretched region when allowed to recover (Fig. 6). The same pattern of changes occurred when we monitored mitochondrial density [Fig. 7(B)]. Thus, it appears that volume addition appears to be temporally coupled to stretch over the course of several hours. This loose coupling of volume addition to lengthening per se was also seen, anecdotally, in cases where the axon increased in caliber while the growth cone was essentially stationary and then thinned when the growth cone rapidly advanced (Supporting Information, Figure 1). These latter observations emphasize that our model is "stretch and intercalation," not necessarily "stretch then intercalation."

To confirm that axonal stretching and growth could occur all along the axon, we towed several neurons from the cell body in the reverse direction to those subjected to tension from the distal end. These experiments (Fig. 8, Table 2, and Video 7) confirmed the earlier results of Campenot (1985) who showed that when the cell body migrated rather than the growth cone, axonal elongation occurred in the proximal region of the axon. Once again, we saw an exponential decay of mitochondrial movements with increasing distance of the mitochondria from the site of tension application. This provides strong support for our interpretation that this pattern is the result of viscoelastic stretching and axonal adhesions, as discussed previously (O'Toole et al., 2008a, b) and is not restricted to the axon near the growth cone. Further, our data indicate that axonal diameter is not static in the proximal region of the axon, increasing our confidence that axonal elongation and growth can occur anywhere along the axon in response to tension.

On the basis of our observations, we suggest the following model for axonal formation (Fig. 9).

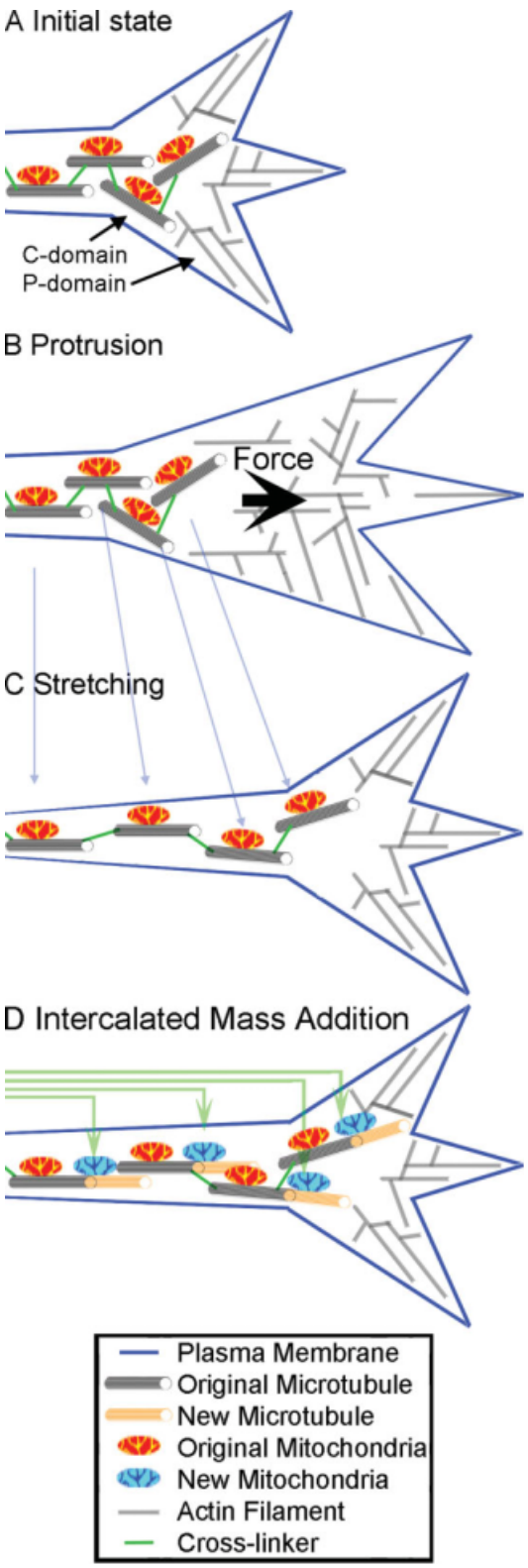

Figure 9 The stretch and intercalation model of axonal formation. A, A diagram of a growth cone with a microtubule/organelle rich region in the central domain and actin rich region in the peripheral domain. B, Protrusion of the leading edge caused by polymerization of the actin cytoskeleton. C, Force generation pulls the central domain of the growth cone forward and causes the axon to stretch. D, New material is added along the length of the axon to prevent axonal thinning. [Color figure can be viewed in the online issue, which is available at www.interscience.wiley.com.]

Tension exerted by the growth cone lengthens the axon by viscoelastic stretching [Figs. 1, 2, 4, and 9(C)]. Stretching occurs at all rates of growth cone advance (Fig. 3), primarily in the distal 100 μm of the axon (Figs. 1, 2, and 4). This pattern arises because adhesions along the axon cause force dissipation (O'Toole et al., 2008a, b). On the scale of minutes, stretching is coupled with thinning of the axon [Figs. 5, 6, 7, and 9(C)]. Over hours, regions undergoing stretching recover their volume [Figs. 5, 6, 7, and 9(D)]. This appears to be a cyclic process where stretching can precede or follow intercalated addition. Although our "stretch and intercalation" model is applicable to axonal growth for peripheral neurons in response to tension, the elongation of different types of axons or elongation in the absence of tension is another matter. Thus, we wish to emphasize that for now our model is confined to tensile regimes of axonal growth of embryonic sensory neurons grown *in vitro*.

The significance of this model for normal axonal development is well illustrated by the normal outgrowth of peripheral neurons from the chick dorsal root ganglia, the source of our cultured neurons. DRG neurons innervating the wing, for example, grow distally several hundred micrometers between E5 and E6 (Hollyday, 1995). During this period, growth cones can be clearly observed, many of which terminate on other axons (Hollyday and Morgan-Carr, 1995). We would postulate that such distal outgrowth would resemble "tip growth" insofar as the tension exerted by the growth cone would extend only to adhesions very near the growth cone, as in Figure 5 where the growth cone advances 500 μm while a branch point remains stationary. However, even in this early stage of chick development, more proximal axonal elongation has been clearly observed. Thus, the distance between two proximal branch points of the developing peripheral nerve in the chick wing increases 300 μm to more than 500 μm (Hollyday, 1995) between E4.5 and E5.5 (Stages 26 and 28) (Hamburger and Hamilton, 1951). Further, during later development (E12) when we isolate neurons from the lumbosacral DRG, the embryo has been growing very rapidly, doubling or tripling in size in the preceding few days while maintaining innervation from the DRG (Sharp et al., 1999). In this case, we would postulate that a whole system of axons undergoes intercalated growth between the DRG and the periphery (e.g., wing or hindlimb) as a result of embryonic growth (Smith, 2009).

This work confirms many aspects of axonal elongation that are well accepted and builds on previous models as discussed above. For example, axons elongate over the course of days without thinning (Bray, 1984), mass addition occurs along the axon (O'Toole et al., 2008a, b), and that large regions of the axon are stationary relative to the substrate (Hirokawa et al., 1997; Chang et al., 1999; Baas et al., 2006). It is interesting to note that stretch leading to a growth response, albeit growth in the context of cell division, is a widely accepted paradigm among surgeons and is known to apply to many different tissue types (De Filippo and Atala, 2002). Our results extend this paradigm to neurons in the context of volume addition. It is well accepted that forces at the growth cone lead to axonal lengthening and are also believed to be critical for axonal guidance. Our work provides a key insight that links forces, lengthening, and presumably guidance together in one model. A prediction of our work is that the proteins that have been identified to be important in axonal guidance (e.g., ena, profilin, ADF/cofilin, α actin, myosin heavy chain, myosin II light chain, CLIP-190, futsch, and short stop) (Sanchez-Soriano et al., 2007) will also be involved in the production or regulation of force generation at the growth cone.

We thank Matthew O'Toole for discussions on the manuscript.

REFERENCES

Abe I, Ochiai N, Ichimura H, Tsujino A, Sun J, Hara Y. 2004. Internodes can nearly double in length with gradual elongation of the adult rat sciatic nerve. J Orthop Res 22:571–577.

Baas PW, Brown A. 1997. Slow axonal transport: The polymer transport model. Trends Cell Biol 7:380–384.

Baas PW, Vidya Nadar C, Myers KA. 2006. Axonal transport of microtubules: The long and short of it. Traffic 7: 490–498.

Bard L, Boscher C, Lambert M, Mege RM, Choquet D, Thoumine O. 2008. A molecular clutch between the actin flow and N-cadherin adhesions drives growth cone migration. J Neurosci 28:5879–5890.

Bernal R, Pullarkat PA, Melo F. 2007. Mechanical properties of axons. Phys Rev Lett 99:018301.

Bray D. 1970. Surface movements during the growth of single explanted neurons. Proc Natl Acad Sci USA 65:905–910.

Bray D. 1973. Branching patterns of individual sympathetic neurons in culture. J Cell Biol 56:702–712.

Bray D. 1984. Axonal growth in response to experimentally applied mechanical tension. Dev Biol 102:379–389.

Brown A. 2003. Axonal transport of membranous and nonmembranous cargoes: A unified perspective. J Cell Biol 160:817–821.

Campenot RB. 1985. The regulation of nerve fiber length by intercalated elongation and retraction. Brain Res 352: 149–154.

Chada S, Lamoureux P, Buxbaum RE, Heidemann SR. 1997. Cytomechanics of neurite outgrowth from chick brain neurons. J Cell Sci 110:1179–1186.

Chan CE, Odde DJ. 2008. Traction dynamics of filopodia on compliant substrates. Science 322:1687–1691.

Chang S, Rodionov VI, Borisy GG, Popov SV. 1998. Transport and turnover of microtubules in frog neurons depend on the pattern of axonal growth. J Neurosci 18: 821–829.

Chang S, Svitkina TM, Borisy GG, Popov SV. 1999. Speckle microscopic evaluation of microtubule transport in growing nerve processes. Nat Cell Biol 1:399–403.

Conde C, Caceres A. 2009. Microtubule assembly, organization and dynamics in axons and dendrites. Nat Rev Neurosci 10:319–332.

Dai J, Sheetz MP. 1995. Axon membrane flows from the growth cone to the cell body. Cell 83:693–701.

De Filippo RE, Atala A. 2002. Stretch and growth: The molecular and physiologic influences of tissue expansion. Plast Reconstr Surg 109:2450–2462.

Dennerll TJ, Lamoureux P, Buxbaum RE, Heidemann SR. 1989. The cytomechanics of axonal elongation and retraction. J Cell Biol 109:3073–3083.

Goldberg DJ, Burmeister DW. 1986. Stages in axon formation: Observations of growth of Aplysia axons in culture using video-enhanced contrast-differential interference contrast microscopy. J Cell Biol 103:1921–1931.

Hamburger V, Hamilton HL. 1951. A series of normal stages in the development of the chick embryo. J Morphol 88:49–92.

Heidemann SR, Lamoureux P, Buxbaum RE. 1999. Mechanical stimulation of neurite assembly in cultured neurons. In: Haynes LW, editor. The Neuron in Tissue Culture. London: J. Wiley and Sons, pp 105–119.

Heidemann SR, Lamoureux P, Ngo K, Reynolds M, Buxbaum RE. 2003. Open-dish incubator for live cell imaging with an inverted microscope. Biotechniques 35:708–714, 716.

Hirokawa N, Terada S, Funakoshi T, Takeda S. 1997. Slow axonal transport: The subunit transport model. Trends Cell Biol 7:384–388.

Hollyday M. 1995. Chick wing innervation. I. Time course of innervation and early differentiation of the peripheral nerve pattern. J Comp Neurol 357:242–253.

Hollyday M, Morgan-Carr M. 1995. Chick wing innervation. II. Morphology of motor and sensory axons and their growth cones during early development. J Comp Neurol 357:254–271.

Kocsis E, Trus BL, Steer CJ, Bisher ME, Steven AC. 1991. Image averaging of flexible fibrous macromolecules: The clathrin triskelion has an elastic proximal segment. J Struct Biol 107:6–14.

Lamoureux P, Buxbaum RE, Heidemann SR. 1989. Direct evidence that growth cones pull. Nature 340:159–162.

Lowery LA, Van Vactor D. 2009. The trip of the tip: Understanding the growth cone machinery. Nat Rev Mol Cell Biol 10:332–343.

Meijering EH, Niessen WJ, Viergever MA. 2001. Quantitative evaluation of convolution-based methods for medical image interpolation. Med Image Anal 5:111–126.

Miller KE, Sheetz MP. 2006. Direct evidence for coherent low velocity axonal transport of mitochondria. J Cell Biol 173:373–381.

Mitchison T, Kirschner M. 1988. Cytoskeletal dynamics and nerve growth. Neuron 1:761–772.

O'Toole M, Lamoureux P, Miller KE. 2008a. A physical model of axonal elongation: Force, viscosity, and adhesions govern the mode of outgrowth. Biophys J 94:2610–2620.

O'Toole M, Latham R, Baqri RM, Miller KE. 2008b. Modeling mitochondrial dynamics during in vivo axonal elongation. J Theor Biol 255:369–377.

Okabe S, Hirokawa N. 1992. Differential behavior of photoactivated microtubules in growing axons of mouse and frog neurons. J Cell Biol 117:105–120.

Pfister BJ, Iwata A, Meaney DF, Smith DH. 2004. Extreme stretch growth of integrated axons. J Neurosci 24:7978–7983.

Popov S, Brown A, Poo MM. 1993. Forward plasma membrane flow in growing nerve processes. Science 259: 244–246.

Sanchez-Soriano N, Tear G, Whitington P, Prokop A. 2007. Drosophila as a genetic and cellular model for studies on axonal growth. Neural Dev 2:9.

Sharp AA, Ma E, Bekoff A. 1999. Developmental changes in leg coordination of the chick at embryonic days 9, 11, and 13: Uncoupling of ankle movements. J Neurophysiol 82:2406–2414.

Shimada T, Toriyama M, Uemura K, Kamiguchi H, Sugiura T, Watanabe N, Inagaki N. 2008. Shootin1 interacts with actin retrograde flow and L1-CAM to promote axon outgrowth. J Cell Biol 181:817–829.

Sinclair GI, Baas PW, Heidemann SR. 1988. Role of microtubules in the cytoplasmic compartmentation of neurons. II. Endocytosis in the growth cone and neurite shaft. Brain Res 450:60–68.

Smith DH. 2009. Stretch growth of integrated axon tracts: Extremes and exploitations. Prog Neurobiol 89:231–239.

Smith SJ. 1988. Neuronal cytomechanics: The actin-based motility of growth cones. Science 242:708–715.

Suter DM, Errante LD, Belotserkovsky V, Forscher P. 1998. The Ig superfamily cell adhesion molecule, apCAM, mediates growth cone steering by substrate-cytoskeletal coupling. J Cell Biol 141:227–240.

Zheng J, Lamoureux P, Santiago V, Dennerll T, Buxbaum RE, Heidemann SR. 1991. Tensile regulation of axonal elongation and initiation. J Neurosci 11:1117–1125.